Passive GNSS-based SAR resolution improvement using joint Galileo E5 signals

Ma, Hui; Antoniou, Michail; Cherniakov, Mikhail

DOI:
10.1109/LGRS.2015.2417594
10.1109/LGRS.2015.2417594

Document Version
Publisher's PDF, also known as Version of record

Citation for published version (Harvard):
Ma, H, Antoniou, M & Cherniakov, M 2015, 'Passive GNSS-based SAR resolution improvement using joint Galileo E5 signals', *IEEE Geoscience and Remote Sensing Letters*, vol. 12, no. 8, 7088585, pp. 1640-1644. https://doi.org/10.1109/LGRS.2015.2417594, https://doi.org/10.1109/LGRS.2015.2417594

Passive GNSS-Based SAR Resolution Improvement Using Joint Galileo E5 Signals

Hui Ma, Michail Antoniou, and Mikhail Cherniakov

***Abstract*—This letter demonstrates the feasibility of improving range resolution in passive synthetic aperture radar with the Galileo navigation satellites as transmitters of opportunity. This can be done by an appropriate coherent combination of the Galileo E5a and E5b signals. The proposed approach is analytically derived and is confirmed both by simulation and experiments.**

***Index Terms*—Bistatic synthetic aperture radar (BSAR), Galileo, global navigation satellite systems (GNSS)-based synthetic aperture radar (SAR), resolution improvement.**

I. Introduction

OVER the recent years, bistatic synthetic aperture radar (BSAR) has seen increased attention from the research community. A BSAR system uses spatially separated antennas for signal transmission and echo reception. This new degree of freedom has given rise to several bistatic configurations using different combinations of transmitter and receiver orientations (i.e., spaceborne, airborne, or fixed) [1]–[3]. In parallel, it has offered the choice of using active systems, with dedicated radar transmitters [4], [5], or passive systems, utilizing transmitters of opportunity such as DVB-T [6], WiFi [7], WiMAX [8], and Global Navigation Satellite Systems (GNSS) [9] for target imaging, among others. This letter focuses on GNSS-based passive synthetic aperture radar (SAR) [10]. In this topology, the transmitter is a navigation satellite like GPS, GLONASS, Galileo, or BeiDou. On the other hand, the receiver can be either fixed on the ground or moving, for example, onboard an aircraft or a ground-moving vehicle. The feasibility of this system has been theoretically and experimentally demonstrated for both moving and stationary receivers [11], [12], as well as using GLONASS [9] and Galileo [12] transmissions.

The benefits in using GNSS as transmitters of opportunity arise from the structure of GNSS networks. GNSS are satellite constellations designed for persistent and global coverage, providing the potential for permanent monitoring [13], [14] anywhere in the world. Furthermore, a single GNSS guarantees that a number of satellites (typically six to eight) illuminate the same area on Earth from multiple angles simultaneously. This offers the possibility to select the optimal bistatic geometry for a given scene, providing the optimal bistatic resolution performance and reducing shadowing effects. It may be also possible to combine bistatic images for terrain classification [15] or to apply multistatic techniques.

The drawback of this technology is that GNSS, as all transmitters of opportunity, were not originally designed for remote sensing, and therefore, they lack the power budget and resolution capability of active systems. To some extent, the power budget and azimuth resolution can be improved by using long dwell times on target. As an example, a coherent processing interval of 5 min may typically provide detection ranges on the order of a few kilometers for buildings or tall trees and an azimuth resolution of 3–4 m. The fundamental bottleneck lies in the range resolution, which depends on the transmitted signal bandwidth and the bistatic acquisition geometry. In a quasi-monostatic configuration, using the GLONASS P-code, the range resolution is 30 m. Using the Galileo E5a or E5b signals, the corresponding range resolution is 15 m, which is still coarse even though twice finer than GLONASS. This coarse resolution capability is a limiting factor to the field of applications for this technology. The problem of spatial resolution is not new to the passive radar community, and efforts have been made to improve it, for example, for DVB-T transmissions [16]. With regard to GNSS specifically, current research investigates the possibility to improve spatial resolution using multistatic signal processing [17]. While this is a powerful technique, offering potential resolution values of $4\ \text{m} \times 4\ \text{m}$ for a fixed receiver and $1\ \text{m} \times 1\ \text{m}$ for a moving receiver, it is geometry specific and introduces artifacts that require additional postprocessing.

This letter investigates the feasibility of improving range resolution in GNSS-based SAR using the Galileo satellites, which may also tackle limitations in BSAR resolution in other research studies [18]. Due to its alternative binary offset carrier (Alt-BOC) signal structure, it is possible to use not just the Galileo E5a or E5b signals individually but also the aggregate E5 bandwidth, which may triple the range resolution to 5 m. However, this is also a complex problem where the traditional technique via a simple coherent summation of the E5a and E5b signals is not suitable. Section II describes the signal structure of the E5 signal and the resulting Galileo-based SAR point spread function (PSF) of a single channel. In Section III, the channel combination concept for the E5 band is introduced and the resolution improvement is confirmed with simulated data of a point target. Finally, Section IV lists experimental methods and results performed to validate the theoretical models.

II. Single-Channel Imaging

The concept of Galileo-based SAR with a fixed receiver is shown in Fig. 1. The transmitter is a Galileo satellite, and the receiver is fixed on the ground. The synthetic aperture is formed by the satellite motion only. The receiver records two signals via two separate channels. The heterodyne channel records

Manuscript received September 18, 2014; revised February 10, 2015; accepted March 24, 2015. This work was supported in part by the Engineering and Physical Sciences Research Council of the U.K. Government under Grant EP/G056838/1 and in part by China Scholarship Council.

H. Ma is with the School of Electronic and Information Engineering, Beihang University, Beijing 100191, China (e-mail: yoyo@ee.buaa.edu.cn).

M. Antoniou and M. Cherniakov are with the School of Electronic, Electrical and Systems Engineering, The University of Birmingham, Birmingham B15 2TT, U.K. (e-mail: m.antoniou@bham.ac.uk).

Color versions of one or more of the figures in this letter are available online at http://ieeexplore.ieee.org.

Digital Object Identifier 10.1109/LGRS.2015.2417594

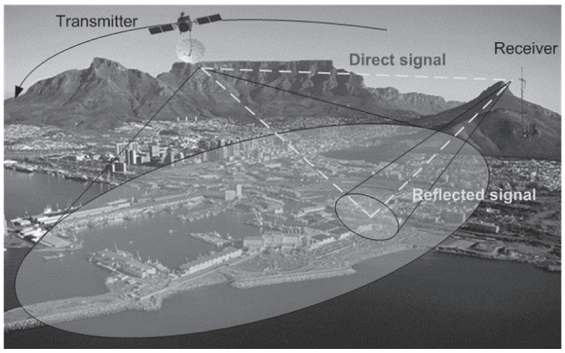

Fig. 1. Concept of Galileo-based SAR.

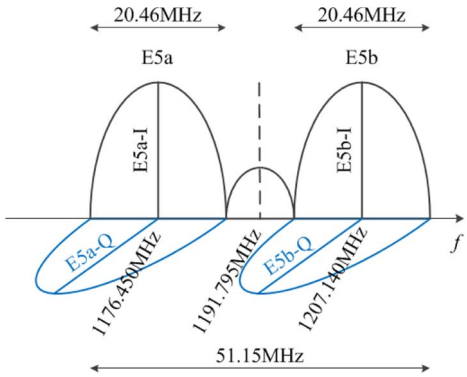

Fig. 2. E5 spectrum representation.

the direct satellite–receiver signal for signal synchronization, whereas the radar channel records satellite signal reflections from an observation area for imaging. The details of the generic signal synchronization and image formation algorithms for this topology are outside the scope of this letter but may be found in [9]. In this section, some of the image formation processes are highlighted assuming Galileo as the transmitting platform.

The transmitted Galileo E5 Alt-BOC signal may be modeled using its alternative linear offset carrier (Alt-LOC) counterpart for simplicity as

$$\begin{aligned} Y(t) = {} & E_{5a-I}(t)D_{aI}(t)\cos\left[(\omega_c-\omega_s)t\right] - E_{5a-Q}(t) \\ & \times \sin\left[(\omega_c-\omega_s)t\right] + E_{5b-I}(t)D_{bI}(t)\cos\left[(\omega_c+\omega_s)t\right] \\ & - E_{5b-Q}(t)\sin\left[(\omega_c+\omega_s)t\right] \end{aligned} \quad (1)$$

where $E_{5a/b-I/Q}(t)$ are the pseudorandom orthogonal codes of the corresponding components with a common chip rate of $f_{\rm cr} = 10.23$ MHz. $D_{aI/bI}(t)$ are the navigation messages of the corresponding in-phase components, whereas the two quadrature signals are data free. ω_c is the carrier angular frequency, and $\omega_s = 2\pi \cdot 15.345$ MHz is the subcarrier angular frequency. Fig. 2 shows the corresponding signal spectrum.

In Fig. 2, it is shown that the E5a and E5b bands are separated, and therefore, it is relatively straightforward to isolate either of these bands for imaging. The most prospective signals are the $-Q$ components of each band as they do not contain any navigation messages, which makes their signal synchronization simpler. Thus, fundamentally, either E5a-Q or E5b-Q channels can be used to extract the scene information. Taking E5b-Q as an example, after quadrature demodulation and SAR data formatting, while ignoring constant phase and amplitude terms,

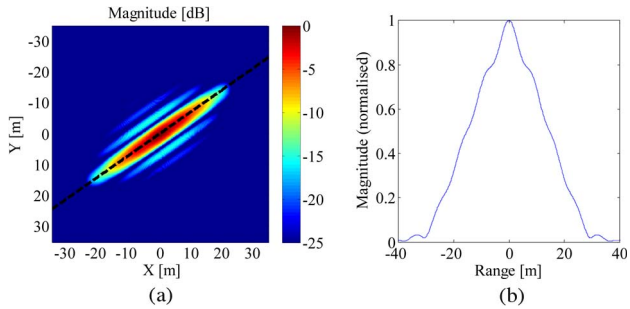

Fig. 3. (a) PSF of the E5b-Q band for a Galileo-based BSAR. The range direction is marked out by the black dotted line. (b) Range cross section of the PSF, indicating a range resolution of 30 m.

the direct and reflected signals from a point target could be written as

$$s(t,u) = E_{5b-Q}\left[t-\tau(u)\right]\exp\left\{j\left[2\pi f_d(u)t + \varphi(u)\right]\right\} \quad (2)$$

where $t \in [0, T_s]$ denotes fast time; T_s is the pulse repetition interval (PRI); $u \in [-T/2, T/2]$ denotes slow time; T is the dwell time on target; and $\tau(u)$, $\varphi(u)$, and $f_d(u)$ are respectively the instantaneous time delay, phase, and Doppler of the reflected signal as functions of u. Assuming perfect synchronization, which tracks $f_d(u)$ [9], the reference signal for range compression can be written as

$$s_0(t,u) = E_{5b-Q}(t)\exp\left\{j\left[2\pi f_d(u)t\right]\right\}. \quad (3)$$

The range compressed data are then given by the correlation function between the reflected signals $s_r(t,u)$ and the complex conjugate of $s_0(t,u)$ as follows:

$$rc_{bQ}(t,u) = \Lambda\left[t-\tau(u)\right]\exp\left[j\varphi(u)\right] \quad (4)$$

with $\Lambda(\cdot)$ being the triangle function centered at $t = \tau(u)$, with a pulsewidth twice that of the E5b-Q chip duration. In terms of the range resolution, it is given in this case by $c/2f_{\rm cr} = 15$ m in the quasi-monostatic case and further degrades as $[c/2f_{\rm cr}\cos(\beta/2)\cos(\theta)]$ due to the bistatic topology, where β is the bistatic scattering angle and θ is the angle between the bisector and ground [10]. Following range compression, data can be focused in the azimuth direction by back-projection [9]. At the output of the back-projection algorithm (BPA), the PSF of the target is obtained. In the range direction, the PSF is a triangular function due to the ranging code correlation properties (4), whereas in the azimuth direction, it is a $\mathrm{sinc}(\cdot)$ function due to the quadratic phase variation of the reflected signal [19]. Fig. 3 presents an example simulated PSF assuming the trajectory and E5b-Q code of a real Galileo satellite (GSAT0104) [20]. In the simulation, $T = 10$ min and $\beta = 90°$, giving a range resolution of approximately 30 m [see Fig. 3(b)], which is rather coarse. At the same time, under this topology, the azimuth resolution may be estimated at approximately 5 m, which is significantly less. Moreover, potentially, the azimuth resolution can be further improved by increasing the dwell time on target, whereas the range resolution is largely specified by the ranging signal bandwidth and is the major bottleneck to the system's resolution capability.

One method of improving the range resolution is to exploit the full E5 band in Fig. 2 rather than a single channel. To do this, the E5b-Q and E5a-Q bands could be coherently combined at the range compression stage. Such a technique has been

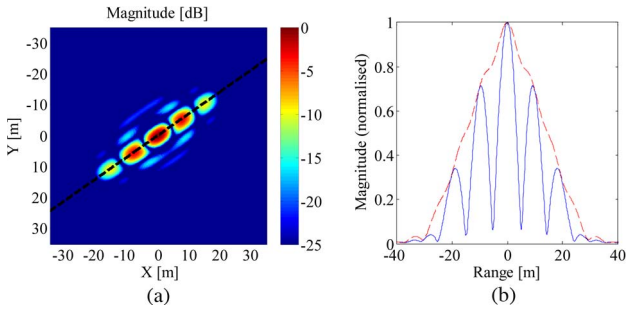

Fig. 4. (a) PSF of the E5b-Q and E5a-Q joint bands for a Galileo-based BSAR. The range direction is marked out by the black dotted line. (b) Range cross section of the PSF, indicating a range resolution of 5 m. The red dotted line is the triangular envelope.

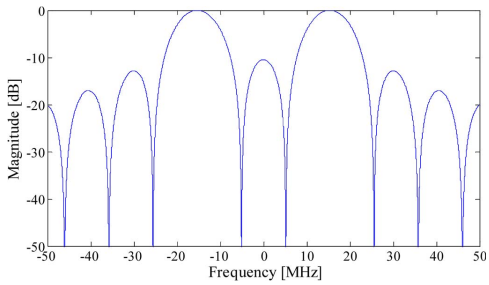

Fig. 5. PSD of coherently combined E5-aQ and E5-bQ correlated signals.

already established by the navigation community to render a better signal tracking performance [21]. Compared with the E5b-Q single-band signal processing, for the E5 full-band case, the local oscillator frequency is centered at the E5 band, and therefore, (2)–(4) can be revised as

$$\begin{aligned} s(t,u) &= E_{5b-Q}\left[t-\tau(u)\right]\cdot\exp\left\{j\omega_s\left[t-\tau(u)\right]\right\} \\ &\quad\cdot\exp\left\{j\left[2\pi f_d(u)t+\varphi(u)\right]\right\} \qquad (5) \\ s_0(t,u) &= E_{5b-Q}(t)\exp(j\omega_s t)\exp\left\{j\left[2\pi f_d(u)t\right]\right\} \qquad (6) \\ rc_{bQ}(t,u) &= \Lambda\left[t-\tau(u)\right]\exp\left\{j\left[-\omega_s\tau(u)+\varphi(u)\right]\right\}. \qquad (7) \end{aligned}$$

Similar to the E5b-Q case (7), the range compressed signal for the E5a-Q band is

$$rc_{aQ}(t,u) = \Lambda\left[t-\tau(u)\right]\exp\left[j\left(\omega_s\tau(u)+\varphi(u)\right)\right]. \qquad (8)$$

Coherently summing (7) and (8), we obtain

$$\begin{aligned} rc_{E5-Q}(t,u) &= rc_{bQ}(t,u)+rc_{aQ}(t,u) \\ &= \Lambda\left[t-\tau(u)\right]\cdot\cos\left[\omega_s\tau(u)\right]\exp\left[j\varphi(u)\right]. \qquad (9) \end{aligned}$$

It is shown in (9) that, after coherent summation, the range correlation waveform is still a triangular waveform but modulated by a cosine waveform. It can be calculated that the resulting waveform has $N = 4\omega_s/2\pi f_{\rm cr}$ lobes, resulting in a six times narrower main lobe. However, the magnitude of the resulting lobes is prohibitively high for remote sensing applications (first lobe is approximately -3.5 dB below the main lobe), and therefore, this technique alone is not enough. To illustrate this, Fig. 4 is the PSF obtained under the same simulation scenario as in Fig. 3 but by applying the coherent combination technique aforementioned. It is also highlighted that these are not sidelobes but are determined by the first two factors of (9), and therefore, traditional sidelobe weighting functions are not applicable either.

III. Channel Combination Concept

The power spectral density (PSD) of the joint signal may be calculated by applying a Fourier transform on (9) as

$$\begin{aligned} G_{E5-Q}(\omega) &= \mathcal{F}\left[rc_{E5-Q}(t)\right] \\ &= \frac{1+\cos(\omega/f_{\rm cr})}{(\omega_s+\omega)^2}+\frac{1+\cos(\omega/f_{\rm cr})}{(\omega_s-\omega)^2} \qquad (10) \end{aligned}$$

where $\mathcal{F}[\cdot]$ denotes the Fourier transform. The PSD is plotted in Fig. 5. It is shown that, similar to Fig. 2, there is a gap between the E5a-Q and E5b-Q bands, which is occupied by signal sidelobes. This is in contrast to other work in the field where the gap between frequency bands is completely unoccupied [16]. The structure of the PSD defines the shape of the correlation function in Fig. 4(b).

The channel combination concept shapes the magnitude of the PSD into a rectangular envelope; thus, the resulting range compression function is a $\mathrm{sinc}(\cdot)$ waveform. The benefit in this approach is that the signal phase needed for azimuth compression remains unaffected since the weighting window alters only the magnitude of the PSD. This technique is similar to spectral equalization principles.

A block diagram of the associated signal processing is shown in Fig. 6. First, the direct/reflected signal is correlated with the coherent summation of the E5a-Q and E5b-Q reference signals, which has already been analyzed in Section II, but without performing the inverse Fourier transform. Second, according to the analytical PSD (10), the weighting window is designed to be the reciprocal of it. By applying the weighting window, the adjusted PSD of the coherently combined E5 signal follows an ideal rectangular envelope. The final step is the inverse Fourier transform. This process is repeated for all PRIs and is performed in the frequency domain so that all targets at different ranges may be corrected in one operation.

At the output of this step, range compressed data have a sinc-like envelope, whose sidelobes may be further reduced with standard weighting functions. These data can be then processed with the same BPA as in the single-channel imaging. Moreover, by this alteration, the effective frequency band is extended to approximately 51.15 MHz, which is the full E5 bandwidth. Compared with single-channel imaging, this yields a range resolution of 3 m in the quasi-monostatic case, which is better than single-channel imaging by a factor of 5.

Fig. 7 shows the simulated PSF with applying the proposed technique under the same simulation scenario as in Fig. 3. Compared with Fig. 4, the peak sidelobe ratio (PSLR) of the compressed signal has been effectively suppressed by the proposed technique. In addition, by implementing the weighting windows, i.e., Kaiser window, the simulated PSLR could be further reduced to -26 dB.

The tradeoff in using this approach is that the spectral equalization process inevitably introduces a certain loss in signal-to-noise ratio (SNR). This loss depends on the extent of the equalizing window since different parts of its spectrum have different power values. Therefore, the wider the window (and the finer the range resolution), the larger the loss. At this stage, it is of interest to calculate the maximum loss, obtained if the full E5 band is to be used. However, it is understood that there is an optimal compromise between resolution and SNR, which is outside the scope of this letter and is part of our future study,

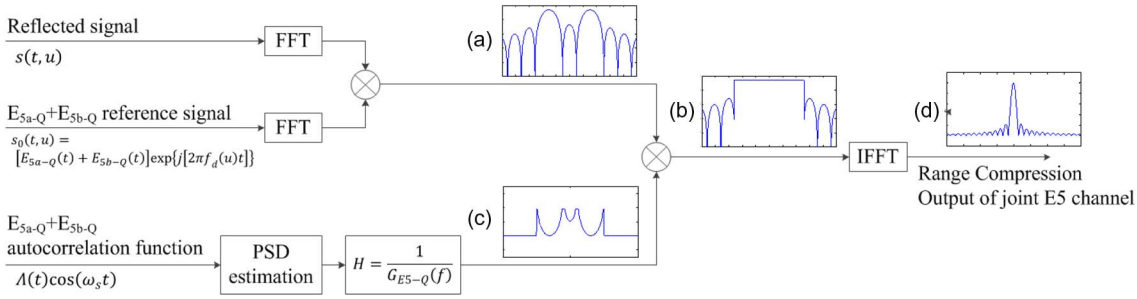

Fig. 6. Channel combination block diagram. (a) Combined E5 PSD. (b) "Equalization" window. (c) PSD after applying the "equalization" window. (d) Correlation function after spectral equalization. (a), (b), and (c) are plotted in unit of "decibels," and (d) is plotted in normalized magnitude.

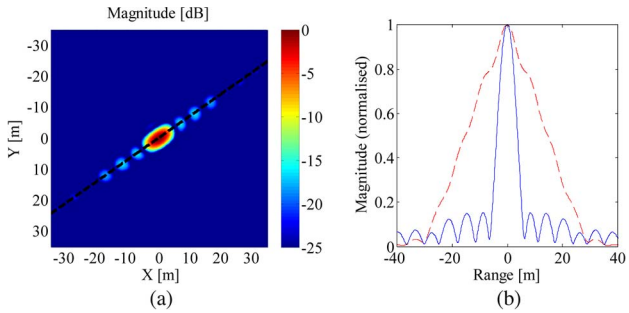

Fig. 7. (a) PSF of the joint E5 channel using the proposed technique. The range direction is marked out by the black dotted line. (b) Range cross section of the PSF, indicating a range resolution of 6 m and a PSLR of -16 dB.

Fig. 8. Experimental hardware.

whereas in this letter, the fundamental feasibility in joining Galileo signal bands is investigated.

The maximum SNR loss may be calculated as the ratio of SNRs with and without spectral equalization

$$\mathrm{SNR}_{\mathrm{loss}} = \frac{\left(\int |S(f) * W(f)|^2\, df\right)}{(E\left[N^2(f)\right] E\left[W^2(f)\right])} \Bigg/ \frac{\left(\int |S(f)|^2\, df\right)}{(E\left[N^2(f)\right])} = \frac{\left(\int |S(f) * W(f)|^2\, df\right)}{\left(\int |S(f)|^2\, df\right)(E\left[W^2(f)\right])} \tag{11}$$

where $S(f)$ is the E5 spectrum,$W(f)$ is the weighting window function, $N(f)$ is the noise spectrum, and $E[\cdot]$ denotes the expected value. Substituting $W(f)$ with (11), the maximum SNR loss of the spectral equalization if the full E5 band is used can be found to be around -14 dB compared with a single channel (taking into account an additional 3-dB gain due to a coherent summation in the channel combination) for a maximum of five times improvement in range resolution. To have a first idea on the effect of this loss on the maximum system detection range, some theoretical calculations can be made based on previous work where the system power budget was calculated [22]. In this letter, it was found that, for a fixed receiver configuration, with 5-min integration time, a 250-m^2 radar cross-section (RCS) target may be detected with a 13-dB SNR threshold up to 21.4 km away from the receiver if a single Galileo channel is used. Taking the SNR loss into account, the new maximum detection range will be approximately 4.3 km. This is a five times reduction in detection range for a five times improvement in spatial resolution. Considering that this system may be better used for local area applications, this reduction in detection range may be traded off for a substantial increase in resolution; however, this example highlights the dependence between maximum range and spatial resolution (directly related to the extent of the equalization window), which is to be investigated further.

TABLE I
EXPERIMENTAL PARAMETERS

Parameter	Quantity	Unit
Transmitter	GSAT0104	--
Carrier frequency	1191.795	MHz
Sub-carrier frequency	15.345	MHz
Transmitted code	PRN20	--
Chip rate	10.23	MHz
Sampling frequency	50	MHz
Pulse Repeat Frequency (PRF)	1000	Hz
Central range	23241	*Km*
Synthetic aperture	1522	*Km*
Bistatic angle	85.6	*Deg*

IV. EXPERIMENTAL VALIDATION

Experiments were made to verify the feasibility of the proposed Galileo E5 combination technique. The experimental hardware (see Fig. 8) of GNSS-based SAR was developed at The University of Birmingham and was able to capture the full E5 signal of a Galileo satellite. At the current stage, PSF is sufficient to verify the proposed technique. To imitate a point target, corner reflectors were not used due to the unexpected RCS under BSAR geometries, whereas one feasible approach is to use two antennas both pointing to the satellite to receive direct signals, one of which is to be considered as a point-like target in the following signal processing, and this configuration has been described in more detail in [17]. In our experiments, the distance between the two antennas was 50 m.

Table I presents the parameters of one set of experiments for GSAT0104 on March 10, 2014, which are similar to the

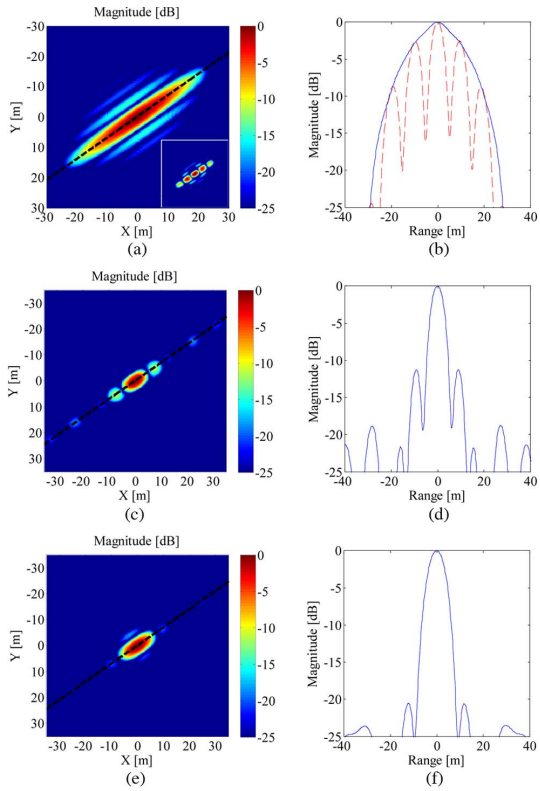

Fig. 9. Experimental results. (a) PSF of the single E5b-Q band. The inset is the coherently combined E5a-Q and E5b-Q band, which uses the same dimensions for the X- and Y-axes and the same color bar. (c) PSF of the combined E5-Q band using the proposed method. (e) PSF after applying Kaiser window upon the range compressed data. The range direction is marked out by the black dotted lines in all PSFs. (b), (d), and (f) are range cross sections of PSFs in (a), (c), and (e), respectively.

simulation scenario in Fig. 7. The data record was 10 min long. The estimated satellite trajectory was obtained from the GNSS satellite tracking website [23] and used to generate the PSF of the point-like target with BPA. First, single-channel imaging was performed as described in Section II with the E5b-Q signal for comparison [see Fig. 9(a)], as well as coherent combination channel imaging for comparison [see the inset in Fig. 9(a)]. Following this, by employing the proposed technique, the PSF of the combined E5-Q band was obtained [see Fig. 9(c)]. The experimental results are in good coincidence with the simulated ones [see Fig. 7(a)] and show that the range resolution is improved from 30 m [see Fig. 9(b)] to 6 m [see Fig. 9(d)] and the PSLR is successfully suppressed. Comparing Fig. 9(d) with Fig. 7(b), the sidelobes are slightly higher in the practical case, but this is expected from a real measurement. In addition, a standard weighting window (Kaiser) was applied to confirm the capability to control signal sidelobes [see Fig. 9(e)]. As a result, there is a broadening of the PSF as always, resulting in a range resolution of 9 m [see Fig. 9(f)]; however, the PSLR reduces to -20 dB.

V. Conclusion

This letter has put forward a resolution improvement proposal for passive Galileo-based SAR. The proposed technique is achieved by coherently combining the Galileo E5a-Q and E5b-Q signals, followed by spectral adjustment to the combined signal. Current results indicate that range resolution can be improved by more than three times compared with the single E5b-Q band at the expense of maximum detection range. Hence, an optimal tradeoff between resolution and SNR loss would be investigated. Our further subsequent work is to test the proposed algorithm on experimental data from real scenes.

References

[1] N. J. Willis, *Bistatic Radar*. Boston, MA, USA: Artech House, 1991.
[2] A. Moccia, N. Chiacchio, and A. Capone, "Spaceborne bistatic synthetic aperture radar for remote sensing applications," *Int. J. Remote Sens.*, vol. 21, no. 18, p. 3395–3414, 2000.
[3] E. Yarman, B. Yazici, and M. Cheney, "Bistatic synthetic aperture radar imaging for arbitrary flight trajectories," *IEEE Trans. Image Process.*, vol. 17, no. 1, pp. 84–93, Jan. 2008.
[4] I. Walterscheid *et al.*, "Bistatic SAR experiments with PAMIR and TerraSAR-X—Setup, processing, and image results," *IEEE Trans. Geosci. Remote Sens.*, vol. 48, no. 8, pp. 3268–3279, Aug. 2010.
[5] F. Behner and S. Reuter, "HITCHHIKER-Hybrid bistatic high resolution SAR experiment using a stationary receiver and TerraSAR-X transmitter," in *Proc. Eur. Conf. Synthetic Aperture Radar*, Jun. 2010, pp. 1–4.
[6] M. Daun, U. Nickel, and W. Koch, "Tracking in multistatic passive radar systems using DAB/DVB-T illumination," *Signal Process.*, vol. 92, no. 6, pp. 1365–1386, Jun. 2012.
[7] P. Falcone, F. Colone, C. Bongioanni, and P. Lombardo, "Experimental results for OFDM WiFi-based passive bistatic radar," in *Proc. IEEE Radar Conf.*, Washington, DC, USA, May 2010, pp. 516–521.
[8] K. Chetty, K. Woodbridge, H. Guo, and G. E. Smith, "Passive bistatic WiMAX radar for marine surveillance," in *Proc. IEEE Radar Conf.*, Washington, DC, USA, May 2010, pp. 188–193.
[9] M. Antoniou and M. Cherniakov, "GNSS-based bistatic SAR: A signal processing view," *EURASIP J. Adv. Signal Process.*, vol. 2013, no. 1, Dec. 2013, Art. ID. 98.
[10] M. Cherniakov, Ed., *Bistatic Radar: Emerging Technology*. Hoboken, NJ, USA: Wiley, 2008.
[11] M. Antoniou, Z. Zeng, F. Liu, and M. Cherniakov, "Experimental demonstration of passive BSAR imaging using navigation satellites and a fixed receiver," *IEEE Geosci. Remote Sens. Lett.*, vol. 9, no. 3, pp. 477–481, May 2012.
[12] M. Antoniou *et al.*, "Passive bistatic synthetic aperture radar imaging with Galileo transmitters and a moving receiver: Experimental demonstration," *IET Radar Sonar Navigat.*, vol. 7, no. 9, pp. 985–993, Dec. 2013.
[13] F. Liu, M. Antoniou, Z. Zeng, and M. Cherniakov, "Coherent change detection using passive GNSS-based BSAR: Experimental proof of concept," *IEEE Trans. Geosci. Remote Sens.*, vol. 51, no. 8, pp. 4544–4555, Aug. 2013.
[14] Q. Zhang, M. Antoniou, W. Chang, and M. Cherniakov, "Spatial decorrelation in GNSS-based SAR coherent change detection," *IEEE Trans. Geosci. Remote Sens.*, vol. 53, no. 1, pp. 219–228, Jan. 2015.
[15] Z. Zeng, M. Antoniou, Q. Zhang, M. Hui, and M. Cherniakov, "Multi-perspective GNSS-based passive BSAR: Preliminary experimental results," in *Proc. 14th Int. Radar Symp.*, Jun. 2013, pp. 467–472.
[16] M. Conti *et al.*, "High range resolution multichannel DVB-T passive radar," *IEEE Aerosp. Electron. Syst. Mag.*, vol. 27, no. 10, pp. 37–42, Oct. 2012.
[17] F. Santi, M. Antoniou, and D. Pastina, "Point spread function analysis for GNSS-based multistatic SAR," *IEEE Geosci. Remote Sens. Lett.*, vol. 12, no. 2, pp. 304–308, Feb. 2015.
[18] A. Moccia and A. Renga, "Spatial resolution of bistatic synthetic aperture radar: Impact of acquisition geometry on imaging performance," *IEEE Trans. Geosci. Remote Sens.*, vol. 49, no. 10, 3487–3503, Oct. 2011.
[19] T. Zeng, M. Cherniakov, and T. Long, "Generalized approach to resolution analysis in BSAR," *IEEE Trans. Aerosp. Electron. Syst.*, vol. 41, no. 2, pp. 461–474, Apr. 2005.
[20] G. J. Undertaking, "Galileo open service. Signal in space interface control document (OS SIS ICD) Draft 1," Eur. Space Agency/Eur. GNSS Supervisory Authority, Brussels, Belgium, Tech. Rep., 2008.
[21] J.-M. Sleewaegen, W. D. Wilde, and M. Hollreiser, "Galileo AltBOC receiver," in *Proc. ENC GNSS*, May 2004.
[22] X. He, *et al.*, "Signal detectability in SS-BSAR with GNSS non-cooperative transmitter," *Proc. Inst. Elect. Eng.—Radar, Sonar Navigat.*, vol. 152, no. 3, pp. 124–132, Jun. 2005.
[23] T. Kelso, "CelesTrak," Public Domain Satellite Tracking Data, 2010. [Online]. Available: http://celestrak.com/